


# SPILLAGE DRAG REDUCTION IN DIVERTERLESS SUPERSONIC INLET

Hajime Miki[1], Junichi Akatsuka[1] & Ren Nimura[2]

[1]Re-BooT Project Team, Aviation Technology Directorate, Japan Aerospace Exploration Agency
[2]Dept. of Mechanical Systems Eng., Graduate School of Eng., Tokyo Univ. of Agriculture and Technology

## Abstract

In aerodynamic design of diverterless inlets characterized by a bump and an inclined cowl, it is challenging to simultaneously suppress boundary layer ingestion and reduce spillage drag. In this study, the effects of a pair of vortex generators installed upstream of the bump on boundary layer ingestion and spillage drag were investigated using CFD analysis. The results indicate that the VG length is a key parameter for reducing boundary layer ingestion. Furthermore, the spillage drag associated with suppressing boundary layer ingestion by VGs is smaller than that achieved by modifying the bump curvature. These findings demonstrate that the application of VGs is an effective approach for designing diverterless inlets with low spillage drag.

**Keywords:** Propulsion/Airframe integration, Supersonic inlet, Boundary layer, Aerodynamic drag, CFD

## 1. General Introduction

To address the challenges of economic efficiency and environmental compatibility in next-generation supersonic passenger aircraft, extensive research and development have been conducted worldwide on both airframe and propulsion systems. Recently, the focus has shifted toward achieving high performance through propulsion/airframe integration design [1]. The supersonic inlet, one of the critical components of the propulsion system, must not only improve propulsive efficiency but also minimize aerodynamic drag and structural weight when integrated with the airframe. One promising approach is the diverterless design, in which the inlet is mounted directly on the airframe surface without utilizing a boundary layer diverter.

A diverterless inlet, characterized by the absence of a diverter, has gained increasing adoption in modern military aircraft [2]. Unlike conventional inlets equipped with ramps or cones as compression surfaces upstream of the inlet, the diverterless configuration employs a bump smoothly blended on the airframe surface. Additionally, the cowl exhibits forward-swept geometry, with its intersection point on the airframe surface located farther aft than the symmetry plane intersection. These features induce spanwise flow turning, effectively preventing ingestion of the boundary layer developed on the airframe surface [3].

Applying diverterless inlets to supersonic passenger aircraft offers potential benefits such as structural simplification and weight reduction by eliminating diverter related components. However, the flow field required to prevent boundary layer ingestion also causes spillage of mainstream flow captured by the inlet. This spillage increases spillage drag, a significant contributor to overall propulsion system drag. Consequently, evaluating diverterless inlet performance requires a trade-off analysis between inlet efficiency and aerodynamic drag. Despite its importance, research on spillage drag characteristics of diverterless inlets remains limited.

The authors have previously conducted a parametric study on the geometries of the bump and cowl, and clarified that, for representative design parameters, a trade-off relationship exists between spillage drag and boundary layer ingestion. Among the parameters considered, widening the entrance width was found to be the most effective in reducing spillage drag while suppressing the increase in boundary layer ingestion [5]. However, achieving further drag reduction requires the introduction of new design concepts or parameters.

https://doi.org/10.71945/icas2026_0418

In previous wind tunnel experiments, it was confirmed that installing a pair of vortex generators upstream of a ramp-equipped supersonic inlet mounted on an airframe in a diverterless configuration improves the aerodynamic performance of the inlet [6].

Based on these findings, the objective of this study is to examine the effectiveness of VGs in the aerodynamic design of a diverterless inlet. To this end, VGs are installed upstream of the bump in a simplified diverterless inlet model, and the effects of VG geometry on boundary layer ingestion and spillage drag are investigated through CFD analysis. The obtained VG effects are then compared with those achieved by varying inlet geometric parameters, and their potential as a technique for reducing spillage drag in diverterless inlets is discussed.

## 2. Design of Bump and Cowl Shape for Spillage Drag Reduction [5]

Figure 1 shows the inlet model used for the parametric study. The inlet is mounted on a flat plate to simulate the approach of the boundary layer from the airframe surface. The bump surface is generated using the conical flow tracing method [4]. The cowl is inclined forward, and its upper surface aligns with a conical shock wave from the bump to prevent mainstream spillage. Meanwhile, its side surface is vertical to the flat plate and positioned inside the shock wave to avoid boundary layer ingestion. The design parameters of the inlet model include the bump curvature, side cowl angle ($\theta_{cowl}$) and capture width ($W_{cap}$). The bump curvature varies by adjusting the tracing height of the conical flow ($K_{bump}$).

Figure 2 shows the baseline shape and the most varied shapes for each design parameter. The baseline shape was designed to produce significant spillage in order to be highly effective at preventing boundary layer ingestion. It features a bump with large curvature, a large cowl angle, and a narrow capture width. In contrast, the comparison shapes were designed to reduce spillage airflow.

Figure 3 illustrates the boundary layer distribution on the bump and flat plate from the RANS results. In Fig. 3(a), for the baseline shape, the approaching boundary layer accumulates on the side of the bump and flows outward upstream of the side cowl. Meanwhile, in Fig. 3(b), for the wider capture case, part of the accumulated boundary layer enters the inlet.

Figure 4 compares the mass flow of the ingested boundary layer and the spillage drag for each inlet shape. The former is evaluated as the ratio of the displacement area to the throat cross-sectional area. The latter is defined as the sum of the pressure drag on the captured flow tube and the variation in drag on the bump and cowl relative to the maximum flow condition. Data corresponding to the same spillage mass flow as the baseline shape are plotted in the graph, and the data points are connected for each design parameter.

As shown in Fig. 4, the mass flow of the ingested boundary layer increases as the spillage drag decreases, regardless of the design parameter. However, the capture width exhibits the smallest rate of increase. Consequently, to reduce the spillage drag of diverterless inlets, the capture surface should be designed as wide as possible while avoiding significant increases in boundary layer ingestion and flow separation.

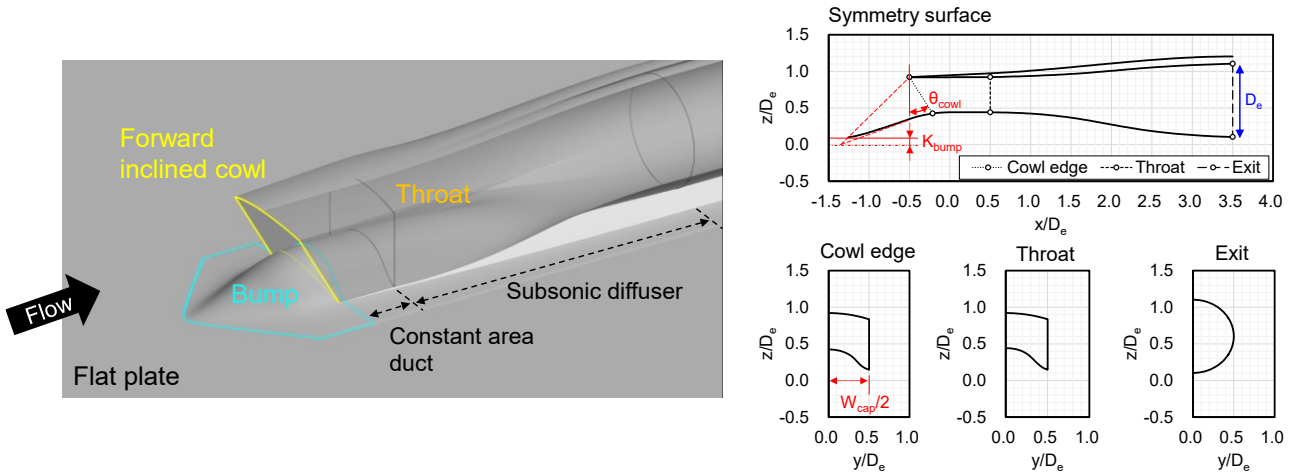



Figure 1 – Inlet model and design parameters.

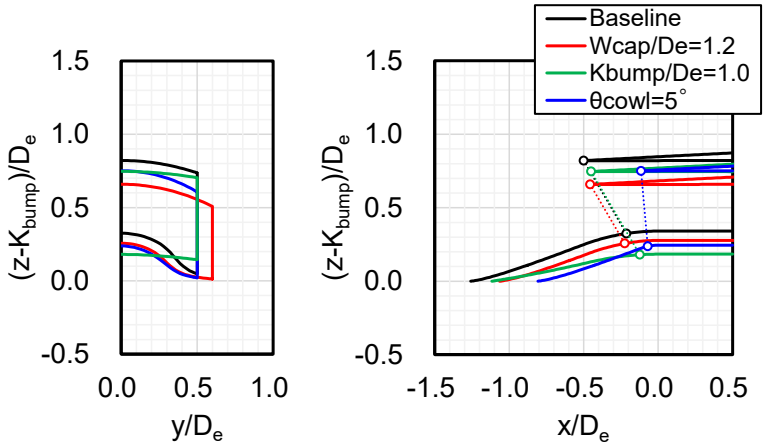
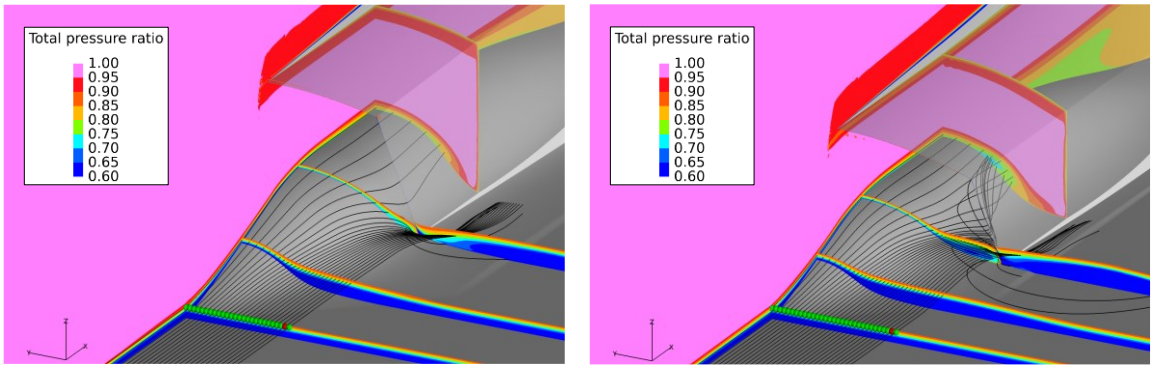



Figure 2 – Bump and cowl shape variation (Baseline: $W_{cap}/D_e$=1.0, $K_{bump}/D_e$=0.1, $\theta_{cowl}$=30°).




(a) Baseline (b) $W_{cap}/D_e$=1.2

Figure 3 – Variation of boundary layer flow with design parameters.

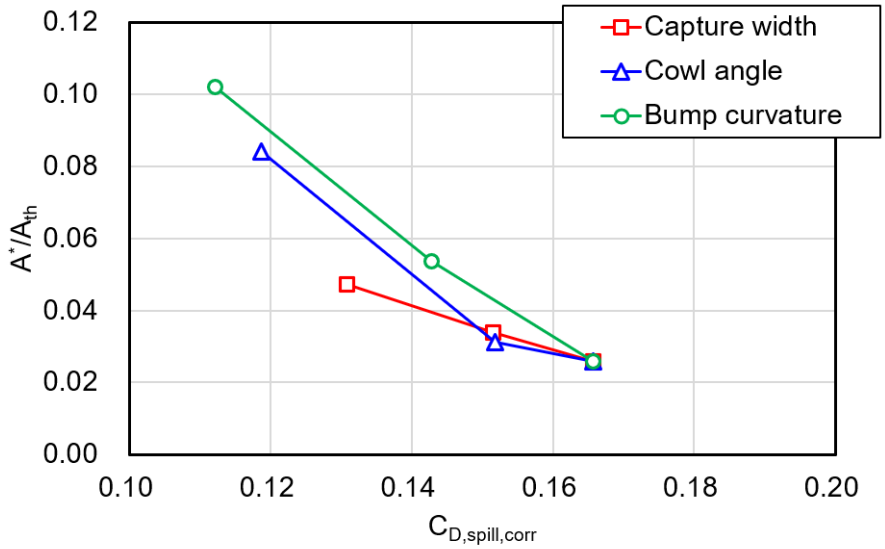



Figure 4 – Effect of design parameters on spillage drag and boundary layer ingestion.

## 3. Application of Vortex Generators Upstream of the Inlet

### 3.1 Concept and Feasibility Test Results [6]

As described in the previous section, the ingested boundary layer increases as the spillage drag decreases. In the case of a wider capture surface, part of the boundary layer collected on the side of the bump does not flow outward. Similarly, a smaller side cowl angle exhibits the same phenomenon, whereas a larger curvature bump does not collect the boundary layer. Therefore, it would be difficult to achieve a significant performance improvement solely by optimizing the bump

and cowl shapes. A combined application of boundary layer control techniques should be considered in parallel.

Figure 5 shows the wind tunnel test setup for the feasibility study. A pair of vortex generators (VGs) were installed symmetrically on the fuselage surface upstream of the inlet with the curved ramp. They are intended to generate counter-rotating vortices and induce spanwise velocity within the boundary layer. The height of the VGs is comparable to the boundary layer thickness, and their installation width is narrower than the capture surface.

Figure 6 shows a photograph of the oil-flow visualization. The streamlines indicate that the VGs generate a pair of vortices at a spacing comparable to their installation width, and the surface flow between the vortices becomes increasingly outward with distance from the VGs. Additionally, the pressure side of the VGs deflects the approaching flow toward the spanwise direction.

The pressure recovery and mass flow ratio of the inlet were evaluated based on the total pressure measurements from the AIP pitot rakes and the flow plug installed downstream of the model. The performances for the cases with VGs installed and the case without VGs (nominal case) are compared in the graph shown in Fig. 7. The wide-VG configuration demonstrates better pressure recovery than the nominal case. Furthermore, the maximum mass flow ratios of both cases are comparable. These results suggest that an appropriate VG layout upstream of the inlet has the potential to mitigate boundary layer ingestion without increasing spillage drag.

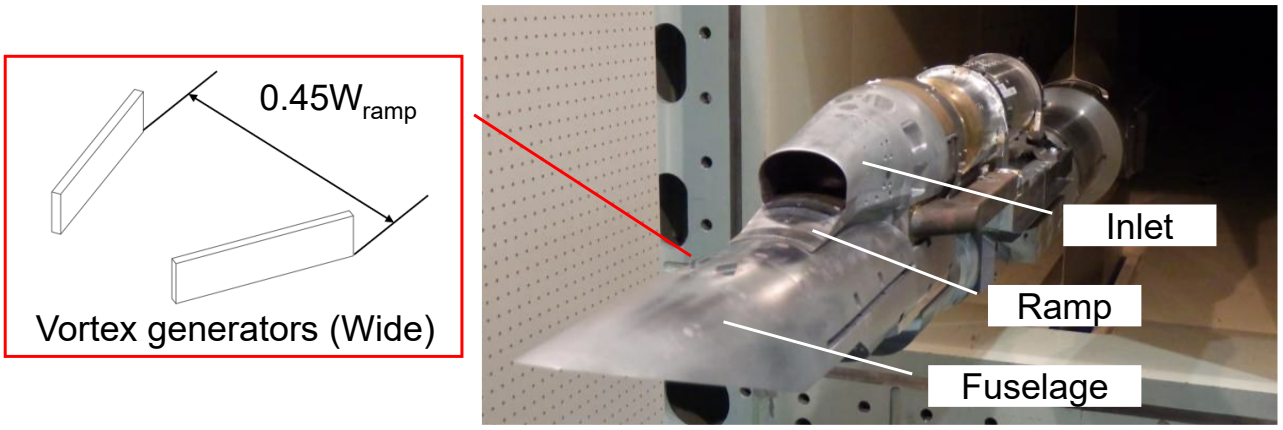



Figure 5 – Wind tunnel test setup for feasibility study of vortex generators.

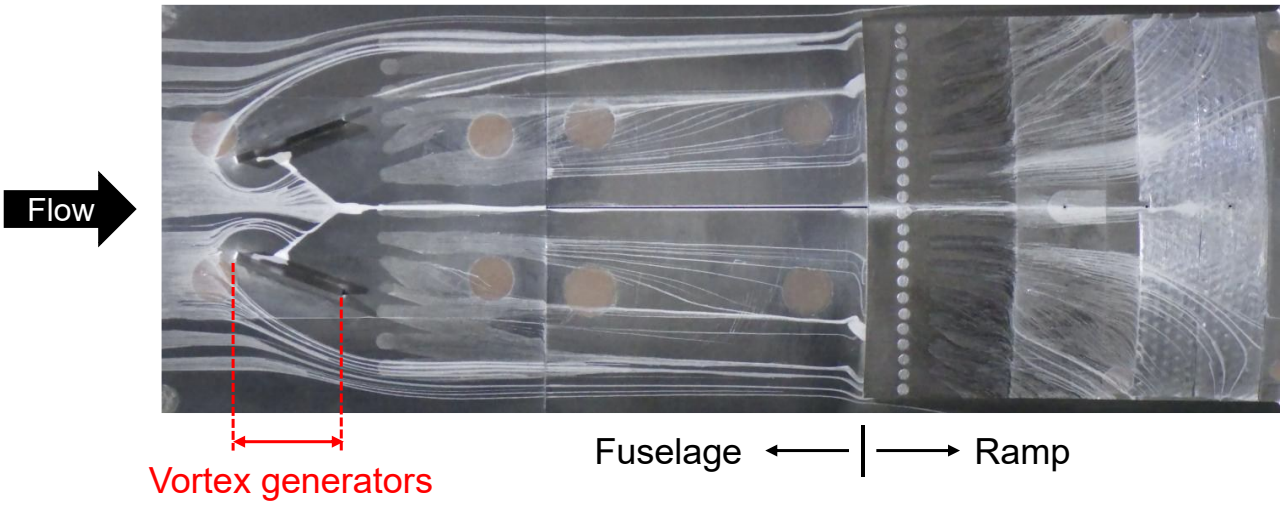



Figure 6 – Oil flow pattern on fuselage and ramp surface.

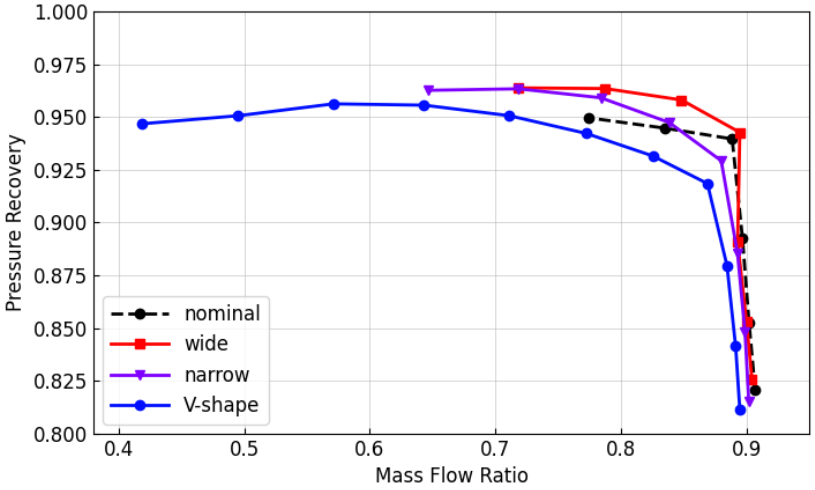



Figure 7 – Inlet performance improvement by vortex generators.

## 3.2 Investigation Method

In the preliminary wind tunnel test, it was confirmed that the inlet performance is improved when a pair of vortex generators (VGs) is installed upstream of an inlet equipped with a ramp. From this section onward, the effects on aerodynamic performance are investigated when VGs are applied to a diverterless inlet, which is characterized by the presence of a bump instead of a ramp. To this end, VGs are placed upstream of the simplified inlet model presented in Chapter 2, and Reynolds-averaged Navier–Stokes (RANS) simulations are performed. The effects of VG geometric parameters on boundary layer ingestion and spillage drag are then evaluated.

### *3.2.1* Inlet Model

Figure 1 shows the inlet model considered in this study. At the entrance, a bump and a forward-swept cowl, which are characteristic features of a diverterless inlet, are employed, and a subsonic diffuser is connected downstream. The design Mach number is 1.6. In addition, the inlet model is mounted on a flat plate for simulating boundary layer ingestion from the airframe. The reference length used in the design is the exit diameter of the subsonic diffuser, $D_e$ .

For the bump, the surface geometry from its apex to the streamwise location of the cowl leading edge on the symmetry plane is defined using a method based on the streamlines of conical flow [4]. The reference conical flow is adjusted according to a geometric parameter, namely the tracing height described later, such that the theoretical mean Mach number behind the oblique shock generated at the bump apex remains constant at 1.26. Furthermore, in order to realign the flow deflected by the bump to be parallel to the freestream, the surface geometry downstream of the cowl leading edge is defined by a circular arc that is parallel to the symmetry plane and tangent to the streamline. The trailing edge of the bump is located $0.1D_e$ downstream of the point where the cowl leading edge intersects the flat plate.

In conventional inlet design, the cowl leading edge is positioned so that it intersects the oblique shock generated by a ramp or cone in order to reduce the spillage flow rate. This configuration is referred to as a shock-on-lip design. However, in a diverterless inlet, if the cowl leading edge is defined along the oblique shock generated by the bump, the capture width becomes larger. As a result, the amount of boundary layer ingestion increases and it becomes more difficult to discharge the ingested flow to the outside of the inlet, making it challenging to maintain inlet performance.

Therefore, in this study, a shock-on-lip design is employed within a certain span from the symmetry plane, while outside this region the design deviates from the shock-on-lip condition, and the cowl leading edge is defined as a straight line perpendicular to the flat plate. The region in which the shock-on-lip condition is maintained from the symmetry plane is referred to as the upper cowl, whereas the region defined by the straight line perpendicular to the flat plate is referred to as the side cowl. The cowl leading edge is a sharp edge, with the inner wall parallel to the freestream and the outer wall inclined at 3° relative to the freestream.

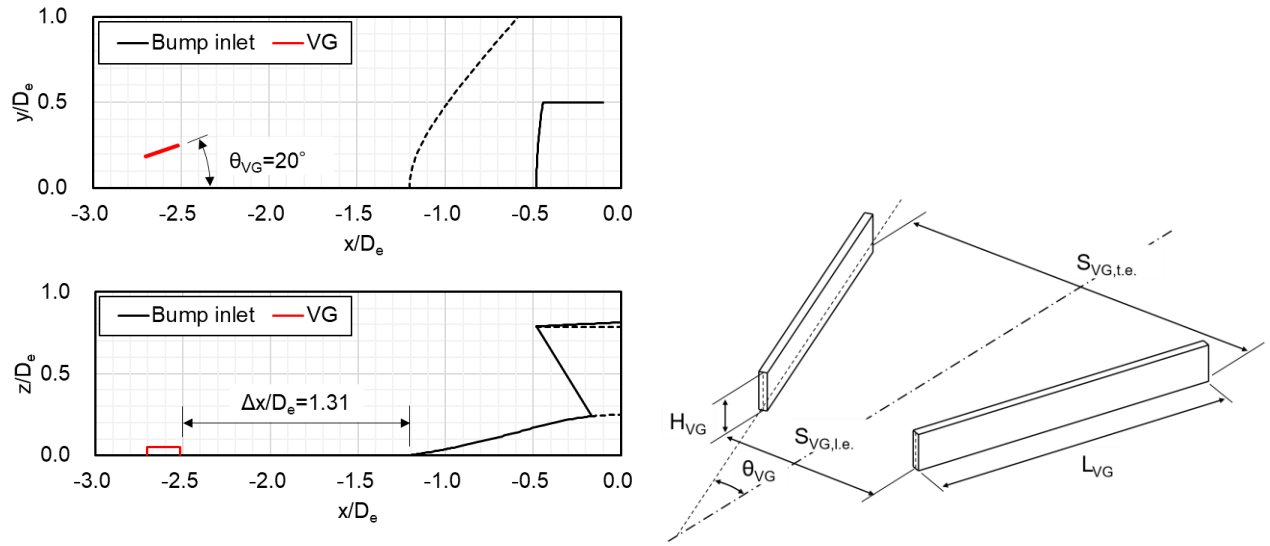



Figure 8 – VG layout and configuration parameters.

Table 1 – Settings of VG configuration.

| | | |
|---|---|---|
| $S_{VG,t.e.}/W_{cap}$ | 0.50 | 0.75 |
| $L_{VG}/H_{VG}$ ($S_{VG,l.e.}/W_{cap}$) | 4, 8, 12 (0.36, 0.23, 0.09) | 8 (0.48) |
| $H_{VG}/D_e$ | 0.05 | |

To allow the flow passing over the bump stabilize before entering the subsonic diffuser, a constant-area duct with a length of $0.5D_e$ is installed downstream of the downstream end of the bump. The cross-sectional shape is kept constant, maintaining the geometry enclosed by the bump and the cowl. The area ratio between the entrance (throat) and the exit of the subsonic diffuser is 1.4, and its length is set to $3.0D_e$.

The geometric parameters of the inlet model are defined as the capture width $W_{cap}$, the cowl sweep angle $\theta_{cowl}$ and the bump tracing height $K_{bump}$, which represents the height at which the conical flow tracing is initiated in the bump design.

The baseline configuration shown in Fig. 1 is designed to have a large spillage flow rate and high effectiveness in boundary layer removal. The parameter values for this configuration are $W_{cap}/D_e=1.0$, $\theta_{cowl}=30°$ and $K_{bump}/D_e=0.1$.

In this study, in order to facilitate the evaluation of the effectiveness of VG application in suppressing boundary layer ingestion, configurations with lower aerodynamic drag but higher boundary layer ingestion compared to the baseline are selected for investigation. Specifically, a configuration with a large bump curvature ($K_{bump}/D_e=0.4$) is considered.

### *3.2.2* VG Configuration

The vortex generators (VGs) placed upstream of the bump are configured as a symmetric toe-in pair with respect to the symmetry plane of the inlet model, based on the preliminary study, in order to achieve suppression of boundary layer ingestion. Figure 8 shows the location of the VGs relative to the inlet model, as well as their geometry and defining parameters.

Based on the preliminary study, the VGs are positioned on the flat plate such that their trailing edges are located $1.31D_e$ upstream of the bump apex. In addition, referring to previous studies, the inclination angle of the VGs relative to the freestream, $\theta_{VG}$, is set to 20°. The VGs are oriented normally to the flat plate on which the boundary layer develops.

The geometric parameters of the VGs are defined as the spacing between the trailing edges of the two VG, $S_{VG,t.e.}$, the length from the trailing edge to the leading edge, $L_{VG}$, and the height from the flat plate surface, $H_{VG}$. In this study, $S_{VG,t.e.}$, $L_{VG}$ and $H_{VG}$ are nondimensionalized by the capture

width $W_{cap}$, $H_{VG}$ and the diffuser exit diameter $D_e$ respectively. The parameter settings are summarized in Table 1.

The nominal configuration is given by $S_{VG.t.e.}/W_{cap}$=0.50, $L_{VG}/H_{VG}$=4 and $H_{VG}/D_e$=0.05. The values of $S_{VG.t.e.}/W_{cap}$ and $L_{VG}/H_{VG}$ are approximately the same as those in the preliminary study where improvement effects were observed. In addition, $H_{VG}/D_e$ corresponds to approximately 0.85 times the boundary layer thickness $\delta_{99\%}/D_e$ at the streamwise location of the VG trailing edge.

To investigate the effects of each geometric parameter, a parametric study based on the nominal configuration is conducted using CFD analysis. When varying $L_{VG}/H_{VG}$, $S_{VG,t.e.}/W_{cap}$ and $H_{VG}/D_e$ are kept constant, and as the VG length increases, the spacing between the leading edges of the two VG, $S_{VG.l.e.}$, becomes smaller. For reference, Table 1 also lists the values of $S_{VG,l.e.}/W_{cap}$.

### *3.2.3* Performance Evaluation Method

To investigate the effects of vortex generators (VGs) on the aerodynamic performance of a diverterless inlet, CFD analyses were performed on inlet models equipped with VGs. The computational mesh generated around the model is shown in Fig. 9.

To obtain aerodynamic performance over a wide operating range from supercritical to subcritical conditions, a second throat was connected downstream of the subsonic diffuser, and multiple CFD simulations were conducted with varying cross-sectional areas of the second throat. The total number of grid points is approximately 6.2 million.

The numerical simulations were carried out using FaSTAR, a high-speed unstructured CFD solver developed by JAXA, on the JAXA Supercomputer System (JSS3). The SA-noft2-R turbulence model was employed.

The freestream conditions in the CFD analyses are a Mach number of 1.6 and a Reynolds number of $1.8\times10^6$, based on the diffuser exit diameter $D_e$. The boundary layer thickness $\delta_{99\%}$ is defined as the distance from the flat plate at which the local total pressure reaches 99% of the freestream total pressure. For the case without VGs, the boundary layer thickness at the bump apex is $\delta_{99\%}/D_e$ = 0.08.

In this study, spillage drag and boundary layer ingestion are evaluated as measures of the aerodynamic performance of the diverterless inlet. The spillage drag coefficient $C_{D,spill}$ is defined as the sum of the aerodynamic force acting on the captured stream tube, $C_{D,spill/gross}$, and the changes in aerodynamic forces acting on the bump and the cowl from the maximum mass flow condition ($\Delta C_{D,bump}$ and $\Delta C_{D,cowl}$). The reference area for the drag coefficient is the maximum capture area of the inlet, $A_c$.

One method for evaluating $C_{D,spill/gross}$ is to obtain the geometry of the captured streamtube by iteratively tracing streamlines that reach the cowl leading edge over its entire span based on the CFD results, and then integrating the pressure over the surface of this streamtube to calculate the aerodynamic force. However, in the present study, vortices generated by the VGs are included in the incoming flow reaching the inlet, making it difficult to accurately determine the captured stream tube and the corresponding aerodynamic force using this method.

Therefore, as shown in Fig. 10, a control volume is defined around the captured stream tube, and $C_{D,spill/gross}$ is evaluated from the balance between the streamwise momentum flux and the aerodynamic forces across the control volume boundaries. The control volume is defined as the space enclosing the captured stream tube within the maximum capture area of the inlet. Based on the momentum equation, the aerodynamic force acting on the captured stream tube, $D_{spill/gross}$, is obtained as follows:

$$D_{spill.gross} = I_{in} - I_{out} - D_{bump,eff} \tag{1}$$

Here, $I_{in}$ and $I_{out}$ denote the impulse functions at the inlet and outlet surfaces of the control volume, respectively, and $D_{bump,eff}$ represents the portion of the aerodynamic force acting on the bump that contributes to the outflow of the captured inlet flow to the outside.

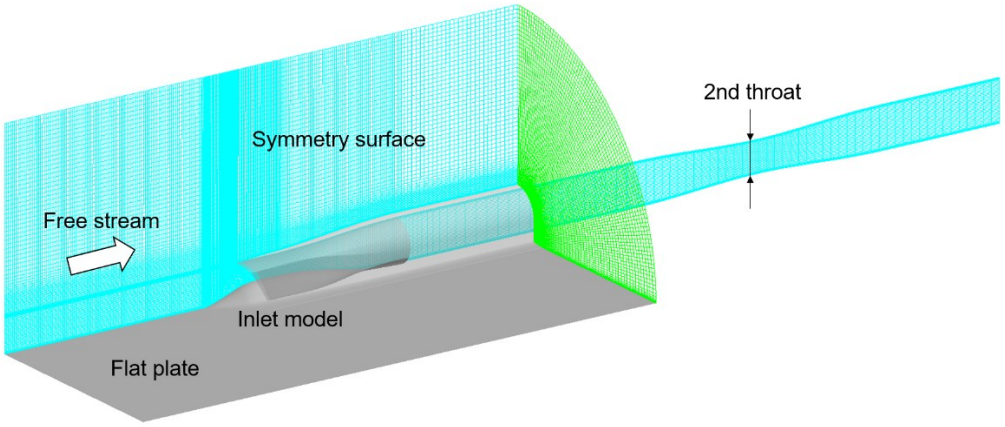



Figure 9 – Computational mesh around the inlet model.

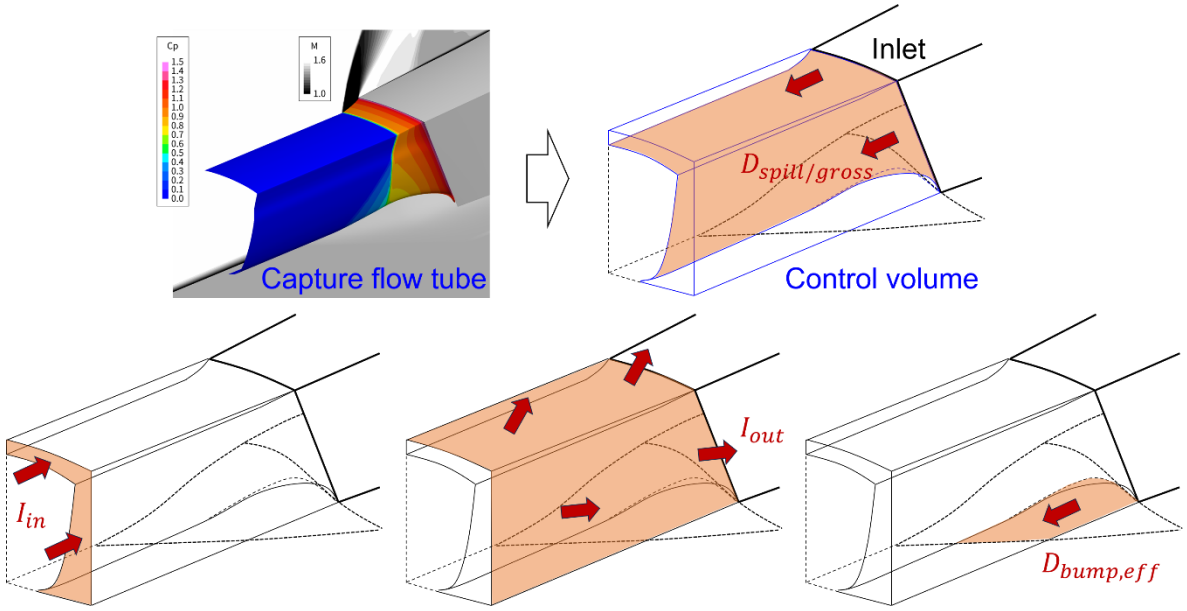



Figure 10 – Control volume for evaluating additive drag.

$I_{in}$ is assumed to be the fraction of the impulse function at the maximum capture cross section upstream of the inlet corresponding to the ratio of the mass flow rate exiting the control volume to the mass flow rate passing through the maximum capture cross section. $I_{out}$ is defined as the sum of the streamwise momentum of the flow exiting through the outlet surfaces, which are defined in the cowl upper-wall and sidewall directions.

Furthermore, it is difficult to identify the region on the bump surface that contributes to the outflow of the boundary layer. Therefore, in this study, it is assumed that the boundary layer outflow occurs within a region whose height is approximately equal to the boundary layer thickness reaching the bump. Accordingly, the aerodynamic force acting on the bump surface within a height of $0.1D_e$ from the flat plate is treated as $D_{bump,eff}$.

The above three components can be expressed as follows:

$$I_{in} = \frac{\dot{m}_{out}}{\dot{m}_{cap}} \int_{A_c} (\rho u)u + \left(p_s - p_{s,\infty}\right) dA \tag{2}$$

$$I_{out} = \int_{A_{out}} \left(\rho \vec{V} \cdot \vec{n}\right)u \, dA \tag{3}$$

$$D_{bump,eff} = \frac{A_{bump,x,z\leq 0.1D_e}}{A_{bump,x}} D_{p,bump} + \frac{A_{bump,z,z\leq 0.1D_e}}{A_{bump,z}} D_{f,bump} \tag{4}$$

In the equations, $\dot{m}$ denotes the mass flow rate, ρ the density, u the streamwise velocity, $p_s$ the static pressure, $\vec{V}$ the velocity vector, and $\vec{n}$ the normal vector. $A_{bump,x}$ and $A_{bump,z}$ represent the projected areas of the bump surface in the $x$- and $z$-directions, respectively. $D_p$ and $D_f$ denote the pressure drag and the friction drag, respectively.

The boundary layer ingestion is evaluated by the ratio $A^*/A_{th}$, where $A^*$ is the boundary layer displacement area at the throat and $A_{th}$ is the throat cross-sectional area. The boundary layer displacement area is calculated by considering the total pressure loss due to a normal shock. The boundary layer is defined as the region extending from the wall to the location where the local total pressure reaches 88.6% of the freestream total pressure. The displacement area is then obtained by integrating the velocity deficit relative to the mean streamwise velocity over the remaining region of the throat cross section.

## 3.3 Results and Discussion

Based on the CFD results, the performance improvement achieved by installing VGs upstream of the bump is examined. First, a comparison is made between the cases with and without VGs under the nominal configuration, and the fundamental changes in the flow field and aerodynamic performance due to the VGs are summarized.

Next, a parametric study of the VG geometry is conducted to identify the geometric parameters with high sensitivity. Finally, the relationship between spillage drag and boundary layer ingestion is comprehensively evaluated, and the potential for reducing spillage drag through the application of VGs is discussed.

### *3.3.1* Effect of VG on the Flow Field and Aerodynamic Performance

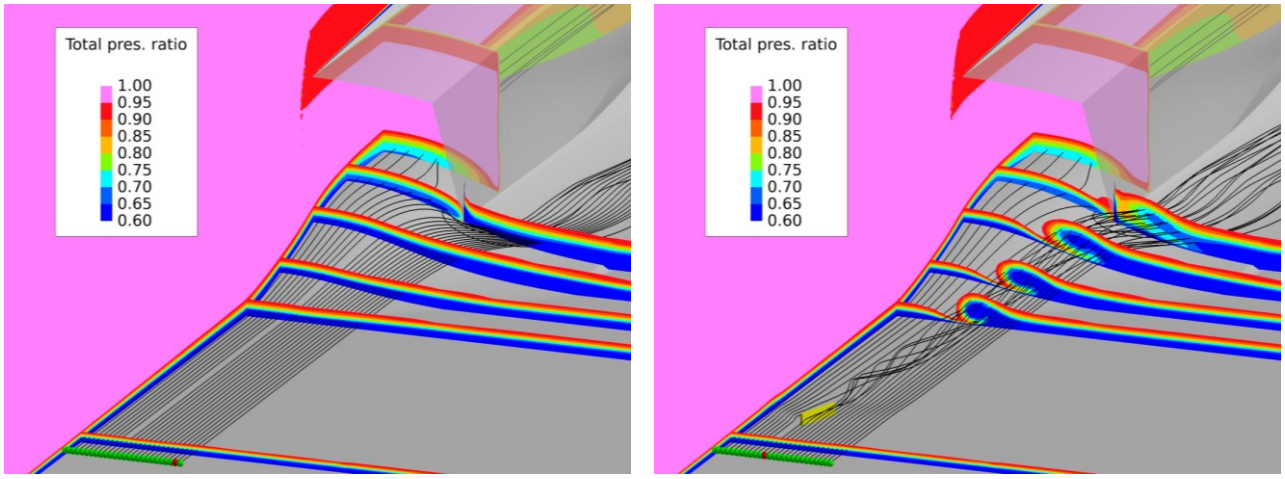
To investigate the changes in the flow field caused by installing VGs upstream of the bump, an inlet model with a larger bump curvature than the baseline, $K_{\mathrm{bump}}/D_e = 0.1$, is considered. Figure 11 shows the flow field around the inlet under nearly identical operating conditions for the cases without VGs (Fig. 11(a)) and with VGs in the nominal configuration (Fig. 11(b)). In this figure, streamlines starting from a height corresponding to half the VG height are visualized from upstream of the VGs. The starting points of the streamlines are uniformly distributed from the symmetry plane to the capture width. In addition, the total pressure ratio distributions at the entrance and at the throat from the bump apex are simultaneously visualized.

A comparison between Fig. 11(a) and (b) shows that the boundary layer reaching the VGs is gathered around the spanwise location corresponding approximately to the VG trailing edges while forming vortices, and is sharply turned, especially in the vicinity of the cowl sidewall, before being discharged to the outside of the inlet. Furthermore, the boundary layer passing between the symmetry plane and the VGs expands in the spanwise direction as it proceeds downstream, filling the region between the symmetry plane and the vortices, and eventually reaches the inlet entrance.

To examine the changes in aerodynamic performance due to the VGs, Fig. 12(a) shows the relationship between the spillage mass flow ratio, $MFR_{spill}$, and the boundary layer displacement area ratio, $A^*/A_{th}$, while Fig. 12(b) shows the relationship between $MFR_{spill}$ and the spillage drag coefficient, $C_{D,spill}$.

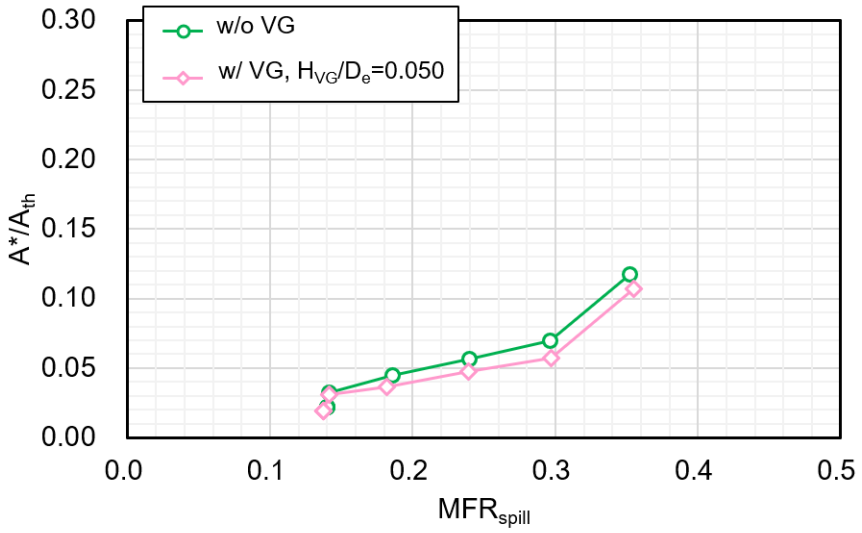
Figure 12(a) indicates that over a wide range of spillage mass flow rates, the boundary layer displacement area ratio is smaller when VGs are installed than when they are not. This implies that the boundary layer ingestion is reduced by the application of VGs. By generating vortices and concentrating the boundary layer near the cowl sidewall, the VGs facilitate the discharge of the boundary layer to the outside of the inlet even with the same bump and cowl geometry.

Next, as shown in Fig. 12(b), the spillage drag increases when VGs are installed. Figure 13 presents the decomposition of the aerodynamic force acting on the captured stream tube, $C_{D,spill/gross}$, into the contributions spilling toward the upper-wall cowl side (Fig. 13(a)) and toward the sidewall cowl side (Fig. 13(b)). These results indicate that the increase in spillage drag due to the installation of VGs is mainly attributed to the increased contribution from spillage toward the sidewall cowl. It is considered that, in order to discharge a larger amount of boundary layer to the outside of the inlet, the flow deflection becomes stronger, resulting in an increase in spillage drag.

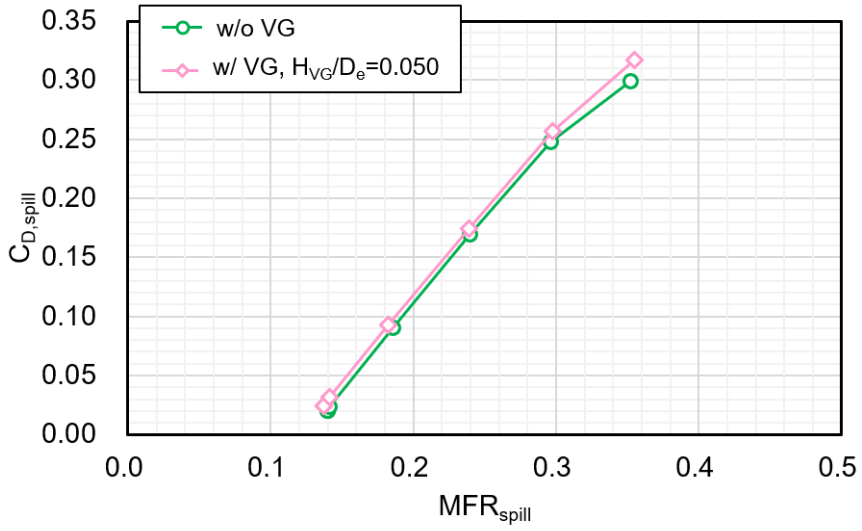



(a) w/o VG (b) w/ VG ($H_{VG}/D_e$=0.050)

Figure 11 – Effect of VG on boundary layer flow
($K_{bump}/D_e$=0.4, $S_{VG,t.e.}/W_{cap}$=0.50, $L_{VG}/H_{VG}$=4).

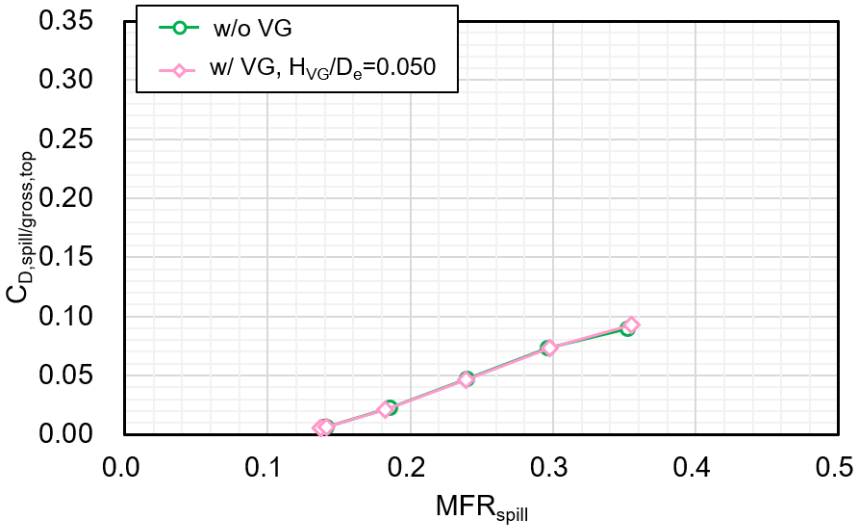



(a) Boundary layer ingestion

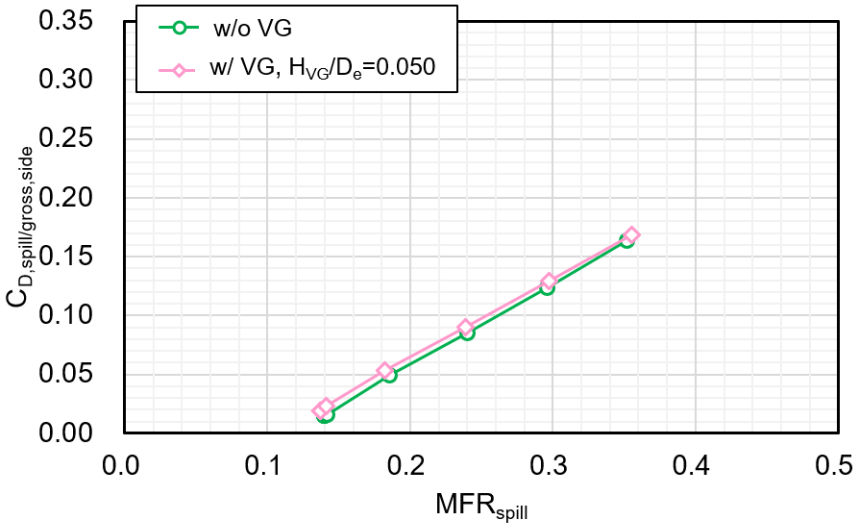



(b) Spillage drag

Figure 12 – Effect of VG ($K_{bump}/D_e$=0.4, $S_{VG,t.e.}/W_{cap}$=0.50, $L_{VG}/H_{VG}$=4).




(a) Upper cowl direction




(b) Side cowl direction

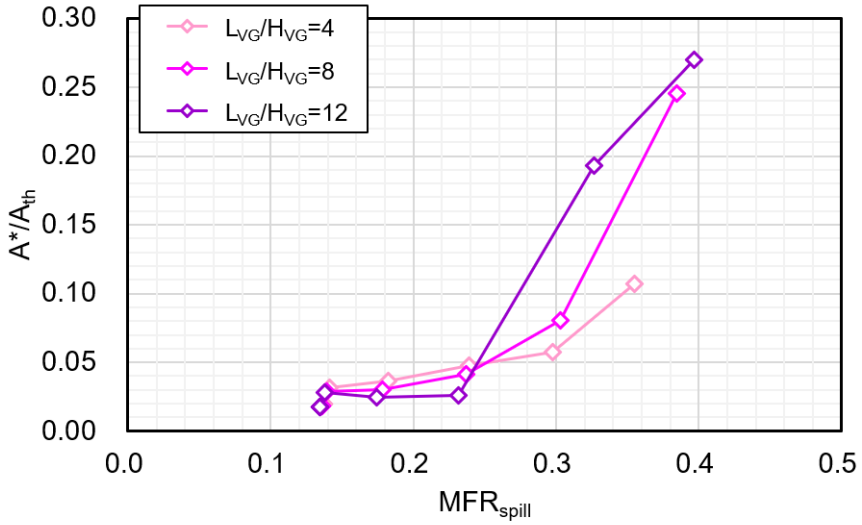
Figure 12 – Spillage drag decomposition by outflow direction ($K_{bump}/D_e$=0.4, $S_{VG,t.e.}/W_{cap}$=0.50, $L_{VG}/H_{VG}$=4).

### *3.3.2* Effect of VG Configuration

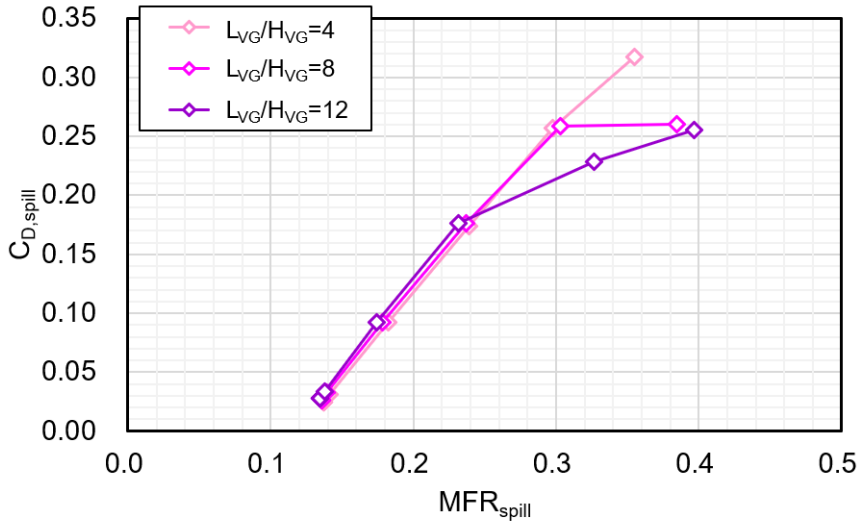
Using the same inlet model as in the previous section, the effects of VG length and spacing on aerodynamic performance are investigated. The aerodynamic performance is evaluated based on CFD results for cases with $L_{VG}/H_{VG}$=4, 8 and 12 for the VG length, and $S_{VG,t.e.}/W_{cap}$=0.50 and 0.75 for the VG spacing. When varying each geometric parameter, the other parameter is kept constant.

Figure 14 shows the variation in aerodynamic performance with respect to the VG length. As shown in Fig. 14(a), the effect of VG length on boundary layer ingestion depends on the magnitude of the spillage mass flow rate. When the spillage flow is small and the inlet operating condition is close to the critical condition, a longer VG results in a lower boundary layer ingestion.

Figure 15 shows the boundary layer distribution around the inlet for $L_{VG}/H_{VG}$=8 and 12. As the VG length increases, the generated vortices become stronger, and the projected width of the VGs in the streamwise direction increases, leading to greater accumulation of the boundary layer downstream of the VG trailing edges. Regardless of the VG length, the accumulated boundary layer is sharply turned just upstream of the cowl sidewall and discharged to the outside of the inlet. Moreover, because the spacing between the VG trailing edges is fixed, the spacing between the leading edges decreases as the VG length increases, resulting in a reduction in the amount of boundary layer passing between the VGs and entering the inlet via the bump.

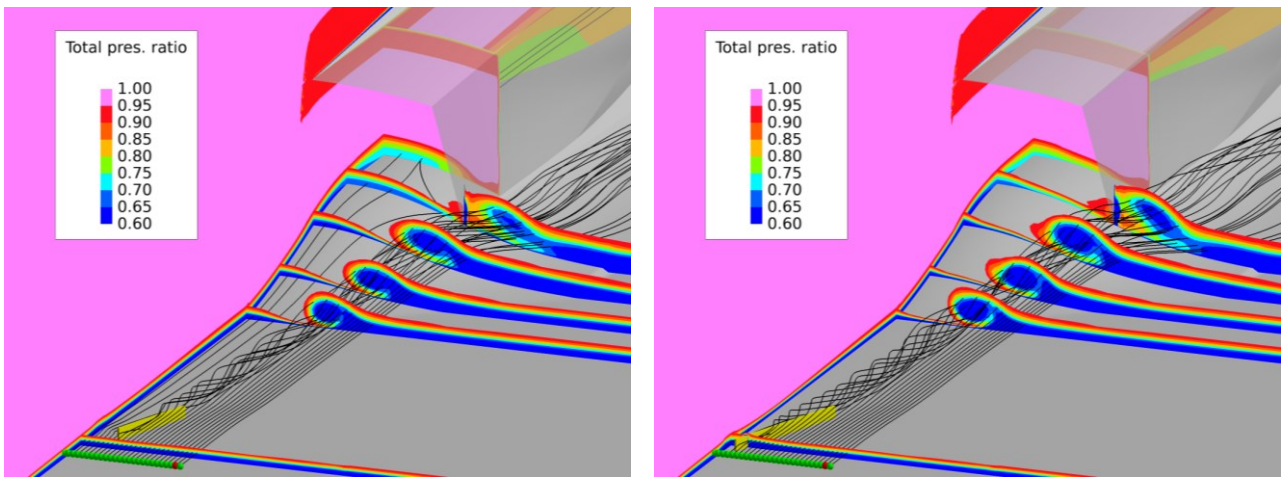



(a) Boundary layer ingestion




(b) Spillage drag

Figure 14 – Effect of VG length ($K_{bump}/D_e$=0.4, $S_{VG,t.e.}/W_{cap}$=0.50).




(a) $L_{VG}/H_{VG}$=8 (b) $L_{VG}/H_{VG}$=12

Figure 15 – Effect of VG length on boundary layer flow ($K_{bump}/D_e$=0.4, $S_{VG,t.e.}/W_{cap}$=0.50).

On the other hand, under subcritical operating conditions with relatively large spillage flow, a larger $L_{VG}/H_{VG}$ leads to flow separation at lower spillage flow rates, resulting in an increase in boundary layer ingestion. This is caused by the locally thicker boundary layer generated by longer VGs, which is more prone to separation through interaction with the terminal shock of the inlet. In this study, the aerodynamic performance near the design point, i.e., under critical operating conditions, is emphasized. Therefore, comparisons under conditions where flow separation occurs are omitted hereafter.

As shown in Fig. 14(b), the spillage drag increases as the VG length increases. This is attributed to the larger flow deflection required to discharge a greater amount of boundary layer to the outside of the inlet.

Next, Fig. 16 shows the variation in aerodynamic performance with respect to VG spacing. In Fig. 16(a), within the range of spillage flow rates where no separation occurs for $S_{VG,t.e.}/W_{cap}=0.50$, it is observed that a larger VG spacing results in increased boundary layer ingestion.

The flow field for $S_{VG,t.e.}/W_{cap}=0.75$ is shown in Fig. 17. The boundary layer accumulated by the VGs is discharged to the outside of the inlet upstream of the cowl sidewall, similar to the case of $S_{VG,t.e.}/W_{cap}=0.50$ (Fig. 15(a)). However, since the spacing between the VG trailing edges is increased while keeping the other geometric parameters constant, more boundary layer passes between the VG leading edges, resulting in a thicker boundary layer distribution over the bump surface and at the inlet entrance.

In Fig. 16(b), the spillage drag decreases as the VG spacing increases. As shown in Fig. 17, the boundary layer accumulated by the VGs is distributed farther from the symmetry plane when the VG spacing is larger compared to the narrower spacing case. As a result, the boundary layer can be discharged to the outside of the inlet with a smaller flow deflection, which suppresses the increase in drag.

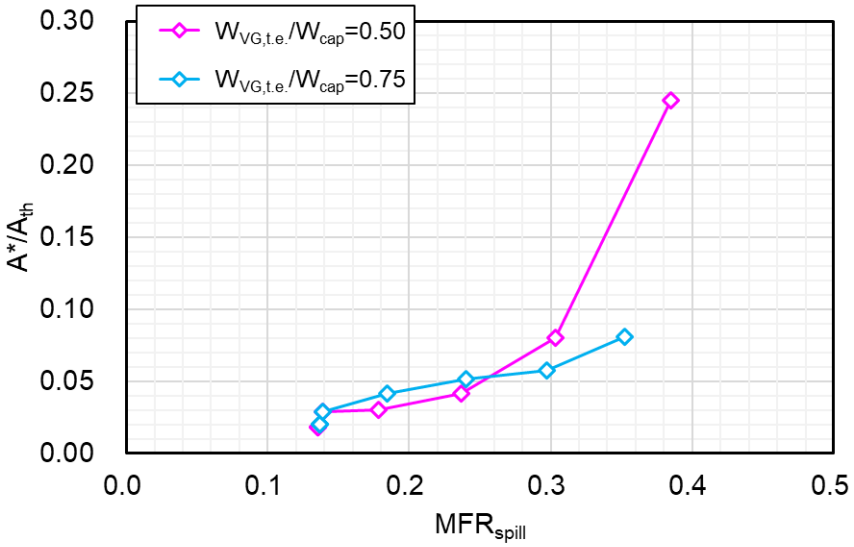
In this study, the objective is to reduce the boundary layer entering the inlet while maintaining low spillage drag by installing VGs upstream of the bump. Therefore, it can be concluded that the VG length is a more key geometric parameter than the VG spacing.

### *3.3.3* Potential for Reducing Spillage Drag

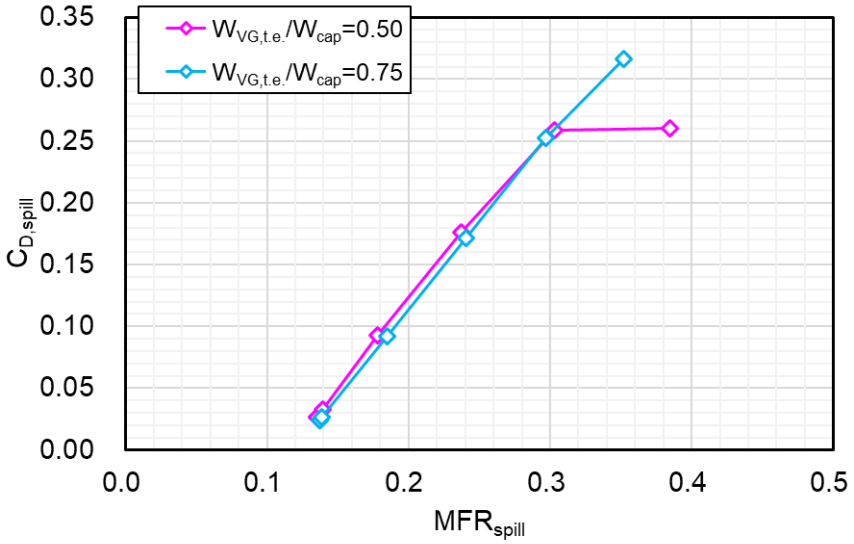
The spillage drag obtained when the boundary layer ingestion is reduced by the application of VGs is compared with that obtained by modifying the inlet geometric parameters. Based on this comparison, the potential for reducing the spillage drag through the application of VGs is investigated. In this section, the effect of VG length is considered as the representative VG parameter. Furthermore, the performance difference between the inlet with a large bump curvature ($K_{bump}/D_e=0.4$), which has been examined in the previous sections, and the baseline inlet with a small bump curvature ($K_{bump}/D_e=0.1$) is treated as the effect of inlet geometric parameters.

In the present inlet model, changes in geometric parameters lead to variations in the maximum capture area. Therefore, even at the same spillage mass flow ratio $MFR_{spill}$, the dimensional spillage flow rate differs. In practical inlet design, the spillage flow rate is largely determined by the engine characteristics. Therefore, the aerodynamic performance is compared under a fixed spillage flow rate. To this end, the maximum capture area of each comparison configuration is adjusted so that the minimum spillage flow rate matches that of the baseline configuration. The spillage drag is also corrected accordingly. The relationship between the corrected spillage mass flow ratio, $MFR_{spill/corr}$, and the corrected spillage drag coefficient, $C_{D,spill,corr}$, is shown in Fig. 18(a), while the relationship with the boundary layer displacement area ratio is shown in Fig. 18(b).

The dashed line in the figure indicates $MFR_{spill/corr}=0.252$, at which the total pressure recovery of the baseline configuration reaches its maximum. The spillage drag coefficient and the boundary layer displacement area ratio for each configuration at this spillage flow condition are obtained by interpolation and plotted together in Fig. 19. In Fig. 19, the data points corresponding to VG application and those corresponding to variation in bump curvature are connected by lines. The clustered point at the left end of the graph represents the aerodynamic performance of the inlet with the smaller bump curvature ($K_{bump}/D_e=0.4$).




(a) Boundary layer ingestion




(b) Spillage drag

Figure 16 – Effect of VG spacing ($K_{bump}/D_e$=0.4, $L_{VG}/H_{VG}$=8).

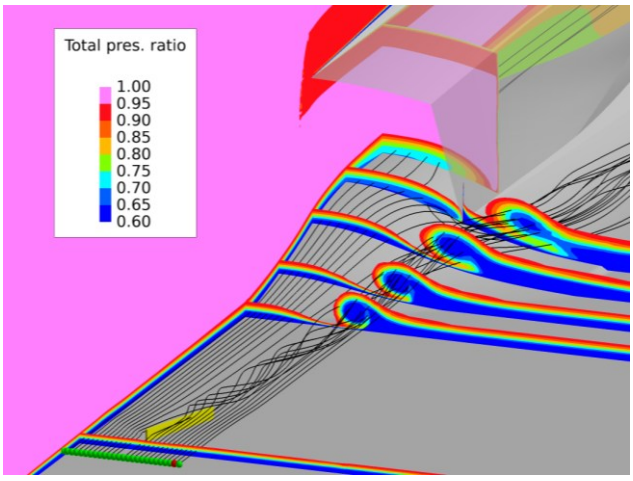
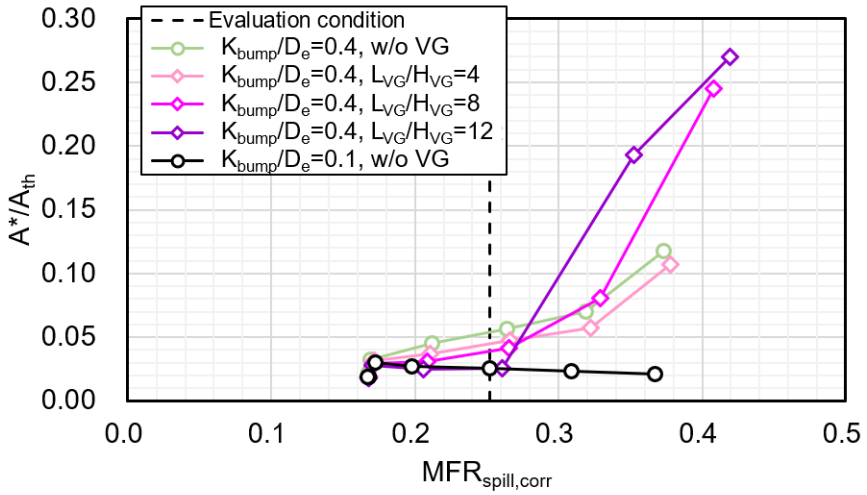



Figure 17 – Effect of VG spacing on boundary layer flow ($K_{bump}/D_e$=0.4, $S_{VG,t.e.}/W_{cap}$=0.75, $L_{VG}/H_{VG}$=8).

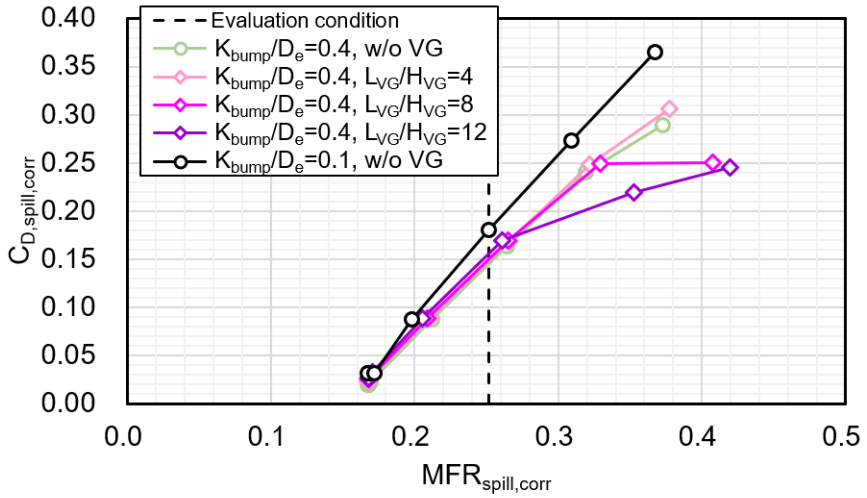
For a given value of the boundary layer displacement area ratio, the spillage drag is lower when VGs are applied. In other words, the application of VGs reduces boundary layer ingestion while suppressing the increase in spillage drag more effectively than changing the bump curvature.

Next, the aerodynamic drag generated by the VGs themselves is examined. The drag of the VGs is considered to be part of the airframe drag, and Fig. 20 shows the sum of the VG drag and the bump drag at the maximum flow condition. Although longer VGs generate larger aerodynamic drag, the bump drag decreases as the VG length increases. As shown in Fig. 21, which presents the pressure coefficient distribution on the bump and the flat plate, the pressure over part of the bump surface is lower when VGs are applied. This is attributed to the locally thicker boundary layer reaching the bump due to the VGs, which suppresses the pressure rise.

As a result of this effect, the increase in the total drag is suppressed, and the difference in drag compared with the case of $K_{bump}/D_e$=0.1 is sufficiently small relative to the variation in spillage drag shown in Fig. 19. Therefore, it can be concluded that the application of VGs provides an effective means of reducing spillage drag.




(a) Boundary layer ingestion




(b) Spillage drag

Figure 18 – Corrected aerodynamic performance ($S_{VG,t.e.}/W_{cap}$=0.50).

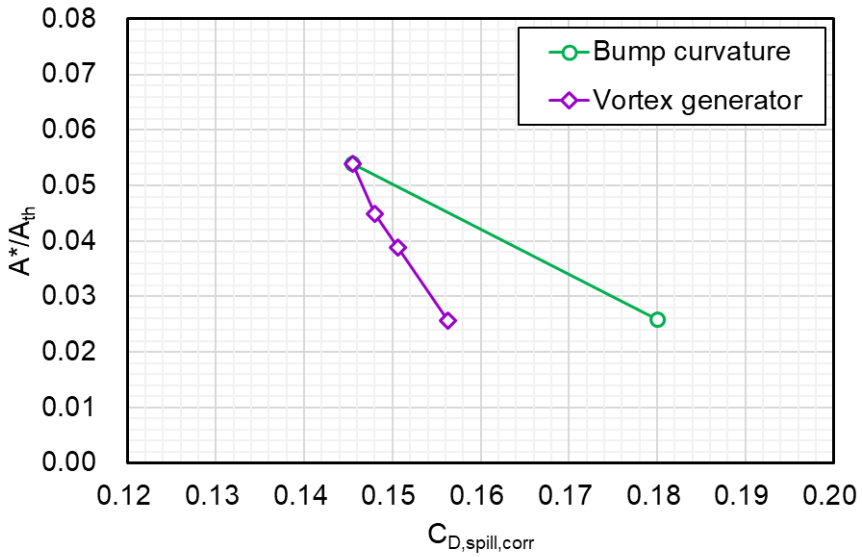



Figure 19 – Trade-off between boundary layer ingestion and spillage drag ($S_{VG,t.e.}/W_{cap}$=0.50).

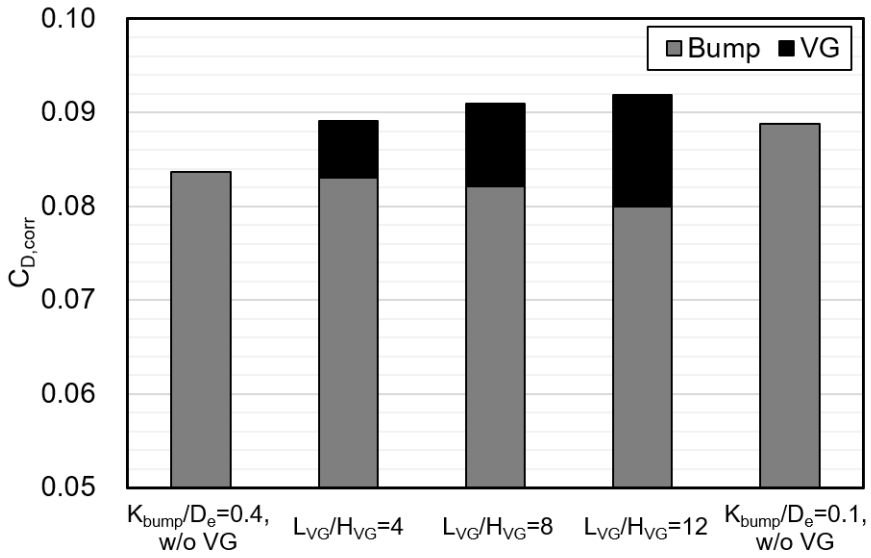
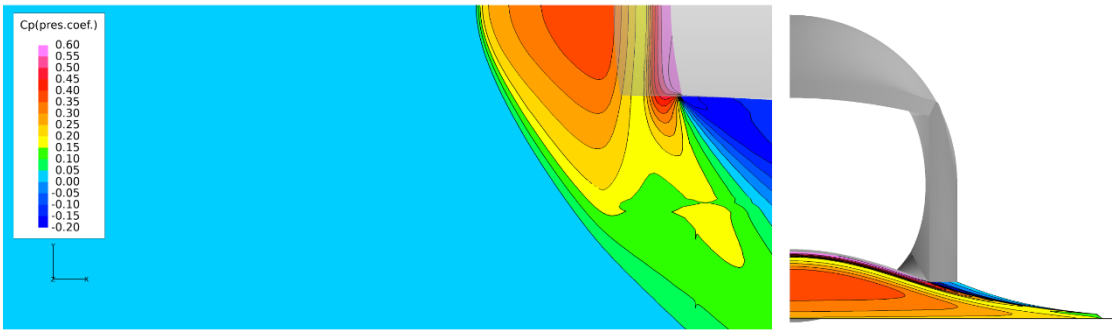



Figure 20 – Airframe drag variation by application of VGs ($S_{VG,t.e.}/W_{cap}$=0.50).

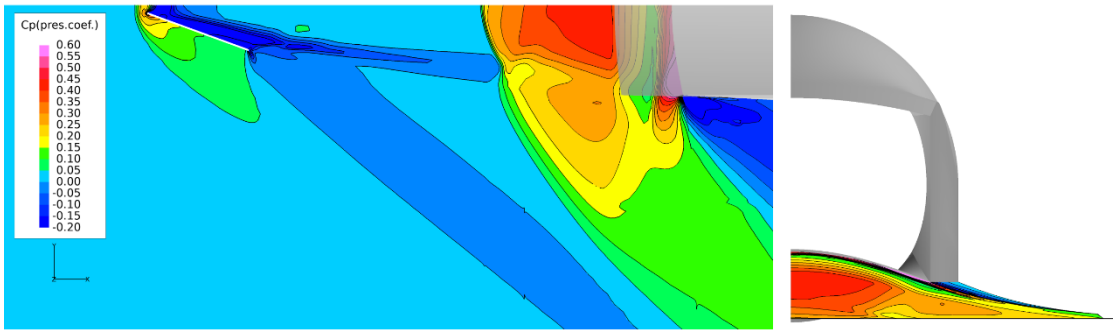
## 4. Conclusion

In this study, CFD analyses were conducted for a supersonic inlet incorporating a bump and a forward-swept cowl, which are characteristic features of a diverterless inlet, with boundary layer ingestion from the airframe simulated. The effects of a pair of vortex generators installed upstream of the bump on boundary layer ingestion and spillage drag were investigated. The results are summarized as follows:

- As the VG length increases, the boundary layer ingestion decreases, while the spillage drag increases.
- To reduce boundary layer ingestion, the VG length is a more important geometric parameter than the VG spacing.
- Compared with reducing boundary layer ingestion by designing a smaller bump curvature, the application of VGs can suppress the increase in spillage drag more effectively.
- Applying VGs upstream of the bump is effective in reducing the spillage drag of a diverterless inlet.




(a) w/o VGs




(b) w/ VGs ($S_{VG,t.e.}/W_{cap}$=0.50, $L_{VG}/H_{VG}$=12)

Figure 21 – Pressure distribution on the bump and the flat plate (left: top view, right: front view).

## 5. Contact Author Email Address

mailto: miki.hajime@jaxa.jp

## 6. Copyright Statement

The authors confirm that they, and/or their company or organization, hold copyright on all of the original material included in this paper. The authors also confirm that they have obtained permission, from the copyright holder of any third party material included in this paper, to publish it as part of their paper. The authors confirm that they give permission, or have obtained permission from the copyright holder of this paper, for the publication and distribution of this paper as part of the ICAS proceedings or as individual off-prints from the proceedings.

## References

[1] Ueno A. and Makino Y., Low-Boom and Low-Drag Design of Small Supersonic Transport Considering Propulsion Airframe Integration, JAXA Research and Development Memorandum, JAXA-RM-18-001E, 2018.

[2] Wiegand C. et.al., F-35 Air Vehicle Technology Overview, AIAA-2018-3368, 2018.

[3] Lockheed Martin Corp., System and method for diverting boundary layer air, US5779189, 1998.

[4] Seddon J. and Goldsmith, E. L., Intake Aerodynamics, AIAA Education Series, 1999.

[5] Miki H., Effect of Diverter-less Design on Spillage drag for Supersonic Inlet, 3A10, Proceedings of the 62nd Aircraft Symposium, JSASS, 2024 (in Japanese).

[6] Nimura R. et.al., Performance Improvement of Supersonic Intake by Vortex Generators Installed Upstream of Compression Ramp, 2D04, Proceedings of the 57th Fluid Dynamics Conference/ the 43rd Aerospace Numerical Simulation Symposium, JSASS, 2025 (in Japanese).